PHYSICAL REVIEW E, VOLUME 64, 015601(R)

Defects and particle motions in the nonuniform melting of a two-dimensional Coulomb cluster

Ying-Ju Lai and Lin I
Department of Physics, National Central University, Chungli, Taiwan 32054, Republic of China
(Received 8 February 2001; published 20 June 2001)

The defect excitation and nonuniform melting of a two-dimensional Coulomb cluster with 300 charged particles (interacting with $1/r$ type force) in a uniform neutralizing background are studied numerically. Intrinsic defects exist around the outer circular shells surrounding the inner triangular lattice. They are the source regions for anisotropic particle thermal vibrations and then cyclic hoppings with the increasing temperature. It leads to the nonuniform melting associated with the thermal motion of intrinsic defects, and then the thermal excitation of dislocation pairs and disclinations. The intrinsic defect free center core has the highest melting temperature. It shows the sequential losses of translational and then orientational orders.

DOI: 10.1103/PhysRevE.64.015601 PACS number(s): 45.05.+x, 64.60.−i, 61.46.+w, 73.23.−b

The two-dimensional (2D) circular Coulomb cluster (2DCCC) consisting of a small number of charged species in a circular symmetric confining potential is a nonlinear mesoscopic system. The recent numerical simulations and experiments have demonstrated many interesting structural and dynamic behaviors [1–10]. The generic packing sequences [2–5], the formation of intrinsic defects (IDs) at zero temperature [3–5], and the eigenmodes for small amplitude collective excitations [6], are the few examples. Nonuniform melting with anisotropic excitations have also been observed numerically by measuring the angular and radial mean kinetic energies, for a few special cases with nonuniform radial particle density distributions [2,4,10]. Nevertheless, the topological behavior and its impact on particle motion and melting have been poorly understood.

Thermal defect (TD) mediated melting has been proposed for the infinite 2D triangular Wigner crystal [11]. For example, in the well known Kosterlitz-Thouless-Halperin-Nelson-Young (KTHNY) scenario for particles with short range interaction [12,13], thermal excitations of free dislocations and then disclinations cause the continuous melting with the sequential losses of the translational and then the bond-orientational orders. The defect density reflects the degrees of spatial disorder [11,13]. For the system with $1/r$ type long range force, the melting scenario is still an open issue. The recent example of a 2D system, with particles sitting on a sphere surface and interacting with $1/r$ type repulsive force, demonstrated that the strain energy of its intrinsic disclinations can be reduced by TD screening. This makes the crystalline state unstable at finite temperature [14]. Obviously, IDs play important roles. Dynamically, the particle motion is strongly related to the local topological structure. The particles around ID regions are less well interlocked than the undistorted lattice regions. Their thermal motions and TDs are easier to be excited [14].

The 2DCCC is the finite N limit of the Wigner crystal, with a large portion of particles nearby the boundary. In general, the 2DCCC with more than a few tens of particles has an inner core with a triangular lattice, surrounded by outer circular shells (e.g., see Fig. 1) [2,4,5]. The lattice distortion causes the formation of IDs mainly in the outer region [5]. Comparing to the above spherical system, the finite circular boundary further reduces the degrees of symmetry and constrains radial motions. It belongs to a different class of systems for testing the melting behavior. In this work, using a model 2DCCC which has 300 particles with $1/r$ type repulsive force as an example, we address defect excitations and their relation with particle motions and nonuniform melting through molecular dynamic (MD) simulation. It is found that the circular boundary and IDs play important roles not only on the outer circular shells and interface regions, but also on the ID-free inner core. The continuous losses of spatial orders mediated by the thermal motions of IDs through particle vibrations, and enhanced by TD generations through the intermediate phase with vortexlike cyclic hoppings are observed for the core melting.

The coupled Langevin-type equations described elsewhere are used in our MD simulation [5]. The equation of motion of particle i (α direction) follows:

$$\frac{d^2x_{\alpha i}}{dt^2} = -\frac{\partial V_i}{\partial x_{\alpha i}} - \gamma\frac{dx_{\alpha i}}{dt} + \eta(x_{\alpha i},t),$$

where the potential V_i of particle i at radial distance r_i consists of the radial confining potential $V_c(r_i)$ and the sum of

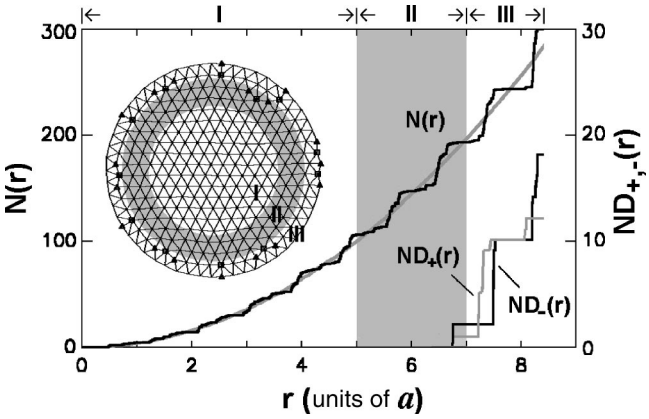

FIG. 1. Cumulated radial distribution of particle number $N(r)$, and the cumulated radial density distribution of defect, $ND_{+,-}(r)$, for the ground state configuration shown in the inset. The gray parabolic curve is the reference for a uniform particle density distribution. The squares and rectangles represent the $+1$ and -1 defects, respectively.

the mutual interaction potential $V_{ij}(r_{ij})$ from particle j at r_{ij} away. $-\gamma(dx_{\alpha i}/dt)$ corresponds to the linear viscous damping to extract kinetic energy to the gas-type background. γ is fixed at 0.05 in the simulation. η is the spatially and temporally δ correlated Gaussian noise with zero mean and variance η_0 to simulate background thermal agitations. All the physical quantities are dimensionless. Only η_0 is varied in this simulation. η_0^2/γ is proportional to the effective temperature [13].

We test the simple case with $V_{ij}=\ln(1/r_{ij})$ and $V_i=r_i^2$ for a 2DCCC at $N=300$. It corresponds to the case with 300 infinite long parallel charged wires sitting in a frozen neutraling background with uniform charge density [5]. Figure 1 shows the ground state configuration of the cluster. The cumulated particle density distribution $N(r)$ mainly falls on a parabolic curve. It manifests the uniform coarse-grained particle density distribution because the system tends to reach a low energy state with zero coarse-grained space charge [5]. This provides a simple starting ground which avoids the complication by the nonuniform radial density distribution as in other forms of interaction and confining potentials [5,6,10].

The ground state cluster has an ID-free core surrounded by two outer circular shells with IDs. For an ordered triangular lattice, the particle inside or on the straight boundary along a lattice line should have six or four nearest neighbors, respectively. The square (triangle) in Fig. 1 represents the $+1$ (-1) topological defect with one more (less) nearest neighbor. IDs are located in the outer region to accommodate the lattice bending. The cluster has -6 net topological charges [5]. According to the radial ID density distribution at $\eta_0=0$, we roughly divide the system into three concentric regions each with 100 particles. Region I is the center defect-free region. Region III is the outmost region with a high ID density. Region II is the transition region that has a triangular lattice structure with a low ID density.

Figure 2(a) plots the η_0 dependences of the averaged defect density $\langle n_{D+,-,I,II,III}\rangle$ in regions I, II, and III, normalized by the number of lattice sites. The $+1$ and -1 defect densities have similar trends except region III is -1 defect rich for lattice bending by the circular boundary [5]. Unlike the mild change of $\langle n_{D+,-,III}\rangle$ around $\eta_0=0.06$ and 0.10, $\langle n_{D+,-,II}\rangle$ and $\langle n_{D+,-,I}\rangle$ exhibit larger but still continuous transitions around $\eta_0=0.08$ and 0.11, respectively. The transition of $\langle n_{D+,-,II}\rangle$ is earlier and less steep than $\langle N_{D+,-,I}\rangle$. Namely, the system exhibits radial dependent melting. Figure 2(b) shows the averaged defect density distributions $\langle n_{D-}(r,\theta)\rangle$ over 2000 t_c, where t_c is the radial oscillation period of the center of mass of the cluster in the confining well (one computing unit = 1/125 t_c). Increasing η_0 causes the earlier azimuthal dominated spread of defects from the localized ID sites and then the radially inward spread to reach a nearly uniform distribution in the liquid state.

Figures 3 and 4 also show the snapshots of the typical defect configurations and the long term particle trajectories at different η_0. At low η_0, the ID free inner domain has a hexagonal shaped boundary (the gray area in Fig. 3), in which particles exhibit isotropic vibrations. In contrast, in the outer circular shells, particles exhibit larger amplitude inter- and intrashell motions associated with the thermal motions of IDs. As η_0 increases, vortexlike cyclic hoppings start around the outer region and then invade to the center part. It generates many TDs and melts the cluster.

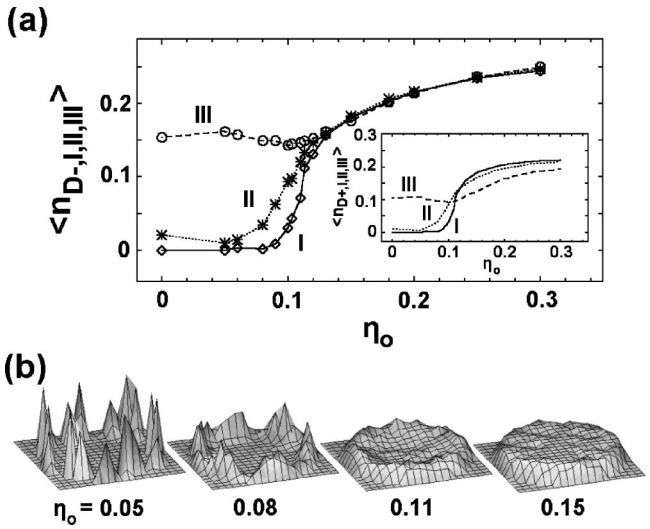

FIG. 2. (a) Averaged number density of -1 defects in regions I, II, and III vs η_0. The inset shows the corresponding $+1$ defect number density. (b) The spatial distribution of the averaged defect density $\langle n_{D-}(\theta,r)\rangle$ at a few different η_0.

The above phenomena can be understood from ID locations and orientations, which are consequences of the symmetry breaking by fitting the hexagonal shaped inner domain

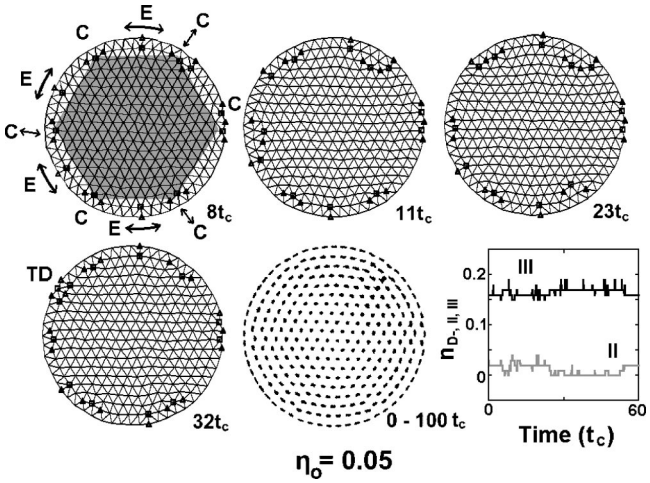

FIG. 3. Typical snapshots indicating the thermal motions of IDs associated with the anisotropic particle motion in the outer regions at low η_0 $(=0.05)$. The temporal evolutions of defect densities in regions II and III are shown in the lower right corner. IDs move along their Burgers vectors (normal to the $+1,-1$ bounds) as indicated by the arrows. The type-*E* IDs move azimuthally (e.g., the ones around the 6, 8, 10, and 12 o'clock positions) between their type-*C* neighbors. The type-*C* IDs around the six corners of the inner gray hexagon can occasionally move radially (e.g., around the 1, 5, and 9 o'clock positions). TDs with paired dislocations are also occasionally generated.

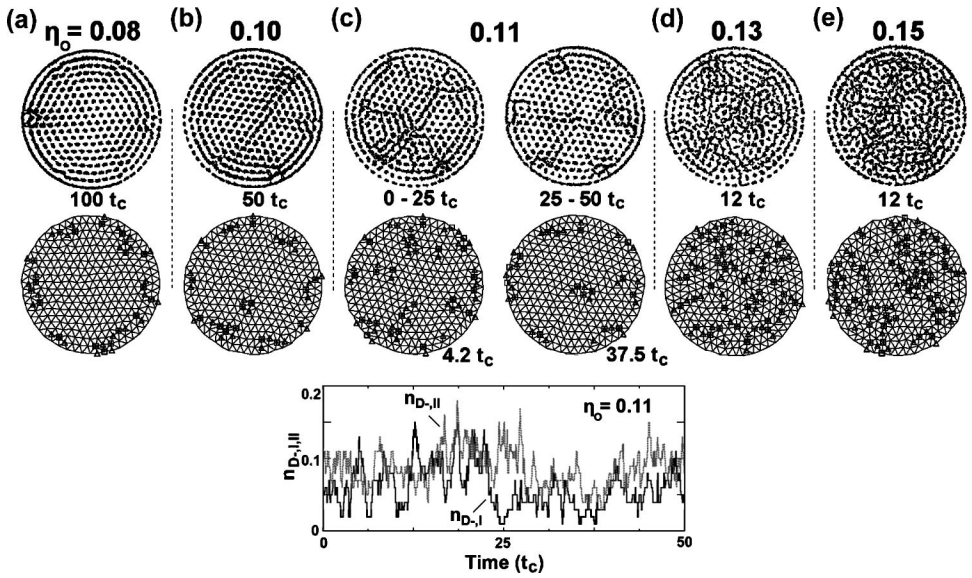

FIG. 4. Typical snapshots of defects configuration and particle trajectories around and after the melting of regions II and I. Paired dislocations, free dislocations, and free disclinations gradually appear in region I. The spatial and temporal scales of cyclic hoppings also gradually decrease. (c) also shows the temporal fluctuations of $n_{D-,I}$ and $n_{D-,II}$.

into the circular outer shells. At low η_0 (<0.08), the azimuthal spread of $\langle n_{D-}(r,\Theta)\rangle$ is mainly from the thermal motions of IDs. According to the defect theory, the excitation energies are low both for the shear-type particle relative motions and the associated dislocation motion along its Burgers vector normal to the $+,-$ bond (as marked by the arrows in Fig. 3) [15,16]. For example, the type-E IDs with $+,-$ defects outside the straight edges of the inner hexagonal domain (e.g., the defects around the 6, 8, 10, and 12 o'clock positions) exhibit azimuthal thermal motion associated with intershell particle azimuthal vibration between their neighboring type-*C* IDs. The motions are sometimes accompanied by the sudden generation of paired dislocations. The type-*C* ID clusters are around the six corners of the inner hexagonal domain, in the form of $-+-$ or $-+-+-$ defect chains. Their radially oriented Burgers vectors pin their azimuthal motions.

The six corners are the source regions for particle radial motions and the inward invasion of disorder. Some IDs in the type-*C* clusters (e.g., around the 1, 5, and 9 o'clock positions) can dissociate and radially move into and out of region II associated with the radial particle vibration around them. Increasing η_0 further induces occasional radial particle hoppings around them. It consequently generates cyclic hoppings, particle azimuthal motions, and TDs in the entire outer region. It leads to the $\langle n_{D+,-,II}\rangle$ transition after $\eta_0 \geqslant 0.08$ [Fig. 2(a)]. The particles in region I also exhibit larger amplitude vibration and the occasional generation of paired dislocation defects [Figs. 4(a) and 4(b)].

For the melting transition of region I around $\eta_0 = 0.11$, cyclic hoppings further extend to region I [Fig. 4(c)]. The type-*C* corners are still the weak areas for radial hoppings. The excitations and reorganizations of hopping vortices at various scales induce generations and annihilations of free and paired dislocations [16]. It causes the fast increase of $\langle n_{D,+,-,I}\rangle$ [Fig. 2(a)], and induces the large fluctuations of n_{D-I} and n_{D-II} over various temporal scales [Fig. 4(c)]. The temporal evolutions of n_{D-I} and n_{D-II} are partially positively correlated in the window of $0.09 < \eta_0 < 0.12$, especially for the low frequency part due to the large scale vortices covering regions I and II. The right part of Fig. 4(c) shows that region I can temporally return to the low defect density state. At larger η_0 (e.g., $\eta_0 \geqslant 0.12$), free-disclinations and more free-dislocations appear in region I, associated with the irregular generation of hopping vortices with smaller scales [Fig. 4(d)]. The lattice lines are seriously distorted. The system enters the disordered liquid state [Figs. 4(d) and 4(e)].

To characterize the translational and orientational orders of region I which is ID free, we further measure the translation pair correlation function $g(r)$ and the bond-orientational function $g_6(r) = \langle \psi_6(0)^* \psi_6(r)\rangle$, respectively (Fig. 5) [11]. $\psi_6(r) = 1/N_i \Sigma_i \exp(i6\theta_i)$, θ_i is the angle of the vector from the particle at r to its ith nearest neighbor, and N_i is the

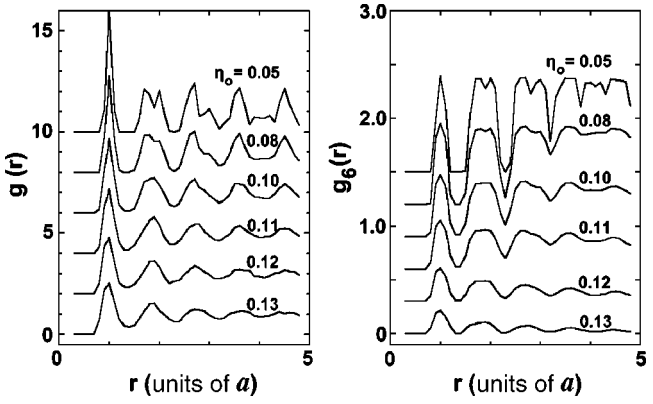

FIG. 5. Correlation functions $g(r)$ and $g_6(r)$ of region I at different η_0. The system shows an earlier loss of the translational order. $g_6(r)$ still has long correlation length at $\eta_0 = 0.11$.

number of the nearest neighbors. Regardless of the earlier gradual loss of the translational order, the orientational order has long correlation length for η_0 up to 0.11. The lattice lines remain quite straight with some free dislocations in addition to the paired dislocations for the transition state at $\eta_0=0.11$. The spatial scaling exponent of $|\langle\psi_6\rangle|^2$ at $\eta_0=0.11$ is 0.26. After $\eta_0=0.11$, the orientation order is lost accompanied by the fast rise of $\langle n_{D+,-,I}\rangle$. Note that the decrease of $|\langle\psi_6\rangle|^2$ with increasing η_0 follows the same type of transition as the increase of $\langle n_{D+,-,I}\rangle$ (not shown). The sequential losses of the translational order and the bond-orientational order associated with the sequential appearance of paired dislocations, free dislocations, and free disclinations are similar to the KTHNY scenario [12]. The easier excitation of TDs extending from the ID regions might be the reason to smooth out the sharp transition found in other 2D systems with $1/r$ repulsive force and finite periodic boundary [17].

The lack of large transition for region III is interesting. It might be due to the suppression of the radial degrees of freedom from the radial confinement and inner core. The slight decrease of $\langle n_{D+,-,III}\rangle$ and the increase of $\langle N_{D+,-,II}\rangle$ while region II melts is due to rounding the corners of the hexagonal domain as the type-*C* IDs move inwards. The inner core induces a more isotropic outward pressure when it loses the orientation order. It makes the outer region form a better circular shell structure with low radial hopping rate at high η_0 [Figs. 4(d) and 4(e)]. Even the third outmost layer, which is piecewise straight at low η_0, has a better chance to form a circular shell. It also causes a lower total defect density than the core.

In conclusion, we study particle motions and melting for a 2DCCC from the views of TDs and IDs. The symmetry breaking by packing a triangular lattice in a circular boundary determines the location and orientation of IDs, and in turn particle collective motions. Particles around IDs are more vulnerable to noise. At low η_0, IDs can thermally move along their Burgers vectors, associated with the anisotropic thermal vibration of particles in the outer shells. As η_0 increases, regions II and I are sequentially melted through the gradual invasions of the larger amplitude vibration and the vortexlike cyclic hopping initiated from the IDs around the six corners of the hexagonal-shaped inner domain. The core enters the transition phase with the loss of the translational order through the generation of paired and free dislocations. It is then followed by the loss of its orientational order through the appearance of free disclination defects, associated with the chaotic small scale cyclic hopping processes. The system finally reaches a liquid state with a more uniform distribution of defects.

This research is supported by the National Science Council of the Republic of China under Contract No. NSC-89-2112-M008-058.

[1] J. J. Thomson, Philos. Mag. **39**, 236 (1904).
[2] V. M. Bedanov and F. M. Peeters, Phys. Rev. B **49**, 2667 (1994).
[3] A. A. Koulakov, F. G. Pikus, and B. I. Shklovskii, Phys. Rev. B **55**, 9223 (1997).
[4] W. T. Juan, Z. H. Huang, J. W. Hsu, Y. J. Lai, and Lin I, Phys. Rev. E **58**, R6947 (1998); W. T. Juan, J. W. Hsu, Z. H. Huang, Y. J. Lai, and Lin I, Chin. J. Phys. (Taipei) **37**, 184 (1999).
[5] Y. J. Lai and Lin I, Phys. Rev. E **60**, 4743 (1999).
[6] V. A. Schweigert and F. M. Peeters, Phys. Rev. B **51**, 7700 (1995).
[7] Y. E. Lozovik and V. A. Mandelshtam, Phys. Lett. A **145**, 269 (1990); **165**, 465 (1992).
[8] D. Z. Jin and D. H. E. Dubin, Phys. Rev. Lett. **80**, 4434 (1998).
[9] R. Bubeck, C. Bechinger, S. Neser, and P. Leiderer, Phys. Rev. Lett. **82**, 3364 (1999).
[10] I. V. Schweigert, V. A. Schweigert, and F. M. Peeters, Phys. Rev. Lett. **84**, 4381 (2000).
[11] K. J. Strandburg, *Bond-Orientational Order in Condensed Matter Systems* (Springer, New York, 1992).
[12] J. M. Kosterlitz and D. J. Thouless, J. Phys. C **6**, 1181 (1973); B. I. Halperin and D. R. Nelson, Phys. Rev. Lett. **41**, 121 (1978); A. P. Young, Phys. Rev. B **19**, 1855 (1979).
[13] P. M. Chaikin and T. C. Lubensky, *Principles of Condensed Matter Physics* (Cambridge University Press, Cambridge, 1995).
[14] M. A. Moore and A. Perez-Garrido, Phys. Rev. Lett. **82**, 4078 (1999).
[15] J. Weertman and J. R. Weertman, *Elementary Dislocation Theory* (Oxford, New York, 1992).
[16] C. H. Chiang and Lin I, Phys. Rev. Lett. **77**, 647 (1996); Lin I, W. T. Juan, C. H. Chiang, and J. H. Chu, Science **272**, 1616 (1996); W. T. Juan and Lin I, Phys. Rev. Lett. **80**, 3073 (1998).
[17] S. W. de Leeuw and J. W. Perram, Physica A **113**, 559 (1982).